Computational Materials Science 50 (2011) 2051–2056

Contents lists available at ScienceDirect

Computational Materials Science

journal homepage: www.elsevier.com/locate/commatsci

Frequency analysis of perfect and defective SWCNTs

Vali Parvaneh *, Mahmoud Shariati, Hamid Torabi

Department of Mechanical Engineering, Shahrood University of Technology, Daneshgah Blvd, Shahrood, Iran

ARTICLE INFO

Article history:
Received 2 December 2010
Accepted 9 February 2011
Available online 5 March 2011

Keywords:
Structural mechanics approach
Frequency analysis
Defective single-walled carbon nanotubes

ABSTRACT

This paper develops a structural mechanical model that analyzes the natural frequency of single-walled carbon nanotubes (SWCNTs) subjected to fixed–fixed and free–fixed boundary conditions. A Morse potential is employed for stretching and bending potentials, and a periodic type of bond torsion is used for torsion interactions. The natural frequencies for various aspect ratios are predicted by this structural model. The effect of different vacancy and Stone–Wales defects on the natural frequency of zigzag and armchair nanotubes is also investigated. Finally, the results of the present structural model are compared with those from other numerical methods.

1. Introduction

The extremely high stiffness and light weight of CNTs results in high vibration frequencies. Due to these features, the vibrational behavior of CNTs is a fundamental characteristic that should be fully studied because it is essential for applications such as NEMS devices. Gibson et al. [1] studied the vibrational behavior of CNTs and their composites, including both theoretical and experimental studies. Using a beam-bending model, Wu et al. [2] investigated the resonant frequency and mode shapes of a SWCNT analytically and through continuum mechanics-based finite element method (FEM) simulations. By using a Timoshenko beam model, Hsu et al. [3] developed a model that analyzed the resonant frequency of chiral single-walled carbon nanotubes (SWCNTs) that were subjected to thermal vibration, including the effect of rotary inertia and shear deformation. They also showed that the frequency increases when the nanotube aspect ratio of length to diameter decreases, and the frequency obtained by the Timoshenko beam model is lower than that calculated by the Euler beam model. Kwon [4] used eigenvalue analysis of mass and stiffness matrices computed from atomistic simulations to predict the natural frequencies and mode shapes of various carbon nanotubes. Xu et al. [5] studied the free vibration of double-walled CNTs modeled as two individual beams by considering van der Waals interactions between the inner and outer tubes. Their methods mainly compute the bending modes of the vibrational modes and natural frequencies. Georgantzinos and Anifanties [6] reported a study of the vibrational characteristics of multi-walled carbon nanotubes modeled exclusively using springs and lumped masses. They examined the effects of different constraints at the nanotube ends on the computed frequencies and mode shapes. By investigating the influence of van der Waals interactions, they concluded that the presence of all corresponding elements is necessary to the vibration analysis of MWCNTs. At the other work [7], they utilized a spring-mass-based finite element formulation for predicting the vibrational behavior of CNTs to investigate their sensing characteristics when a nanoparticle is attached them. They found that the combination of frequency shifts of the basic modes could provide a basis for the ability to not only sense an added mass, but also determine its weight and position on the CNT. Li and Chou [8] discerned the effects of tube diameter, length and end constraints on the fundamental frequency using a molecular structural mechanics model with beam elements. Chowdhury et al. [9] investigated the vibrational properties of zigzag and armchair SWCNTs using the molecular mechanics approach. Their results showed features of decreasing frequencies (on the first five vibration modes) with increase in aspect ratio. They also found that the frequency of SWCNTs is primarily determined by the geometric sizes (diameter and aspect ratio) but cannot be substantially changed due to variation of their atomic structures. Hashemnia et al. [10] investigated the vibrational properties of two kinds of single-layered graphene sheets and single-wall carbon nanotubes (SWCNT) using a molecular structural mechanics approach. Their results indicated that the fundamental frequency decreases as the aspect ratio increases, and the fundamental frequency of nanotubes is larger than that of graphene sheets. Mir et al. [11] and Sakhaee-Pour et al. [12] investigated the vibrational behavior of bridge and cantilever SWCNTs with different lengths and diameters. Both of them used a finite element method with beam elements in their simulations.

Most of the existing papers have obtained natural frequencies of CNTs with high aspect ratios. For small aspect ratios, the values of natural frequencies are higher and are often used in nano-electro-mechanical systems (NEMS). Hence, the exact prediction of natural frequencies at this range seems to be necessary. Furthermore,

* Corresponding author. Tel.: +98 915 1014452.
E-mail address: vali.parvaneh@gmail.com (V. Parvaneh).

0927-0256/$ - see front matter © 2011 Elsevier B.V. All rights reserved.
doi:10.1016/j.commatsci.2011.02.007

existing differences between the observations are at the shell mode. At small aspect ratios with the fixed–fixed boundary conditions, the shell mode usually occurs. Therefore, using of an exact model to predict natural frequencies is of a great importance. In the work of Li and Chou [8], values of natural frequency for aspect ratios equal to 6 and higher were only presented. Thus, the results were obtained exactly for the range of the Euler mode. Their results for the Euler mode are in agreement with the present work.

The work of Mir et al. [11] and Sakhaee-Pour et al. [12] was also extended to the high aspect ratios. The results of Hashemnia et al. [10] were obtained for small aspect ratios. The small difference in the results for the Euler mode is related to the different inter-atomic interactions in the models that were assumed. However, noticeable differences in the shell mode can be described as solely due to the inter-atomic interactions. It is obvious that a beam model is incapable of predicting the natural frequencies of the shell mode due to differences in the actual nature of the bending interactions of CNTs that cannot be satisfied in the beam model whenever the shell mode occurs. In fact, the beam-bending means that C–C bonds will be bent far from reality. This can be acceptable for prediction of Young's modulus but it does not yield logical results for prediction of natural frequencies. In the present model, the angle variation potential is modeled by an axial spring with values nearer to the reality (C–C bonds will not be bent). As discussed in predicting the buckling of CNTs in the work of Parvaneh et al. [13], at the same time, a beam model cannot predict the critical buckling load and the buckling mode for different aspect ratios. This problem is obvious in the work of Hashemnia et al. [10], where they obtained natural frequencies for aspect ratios lower than 6. However, if Mir et al. [11], Sakhaee-Pour et al. [12], and Li and Chou [8] had explored their results for small aspect ratios, the same problem would have been created.

Here, we studied frequency analysis of fixed–fixed and free–fixed SWCNTs with different aspect ratios (L/D) and compared their frequencies with those of other methods. Therefore, in this work a structural mechanics model (Parvaneh et al. [13]) was employed to determine the natural frequencies and their corresponding modes for two types of SWCNTs, i.e., zigzag and armchair.

2. Simulation method

2.1. Application of the structural model to SWCNTs

We have proposed a structural mechanics method to model the carbon nanotubes. The detailed derivation procedure for the formulation and other features of this model can be found in our previous work (Parvaneh et al. [13]).

The total steric potential energy due to interactions between carbon atoms can be represented by Eq. (1) [14]:

$$u_{total} = u_r + u_\theta + u_\phi + u_\omega \tag{1}$$

where u_r, u_θ, u_φ, and u_ω are bond energies associated with bond stretching, angle variation or bond bending, dihedral angle torsion, and out-of-plane torsion, respectively.

In this model, Morse potentials are employed for stretching and bending potentials, and a periodic type of bond torsion is applied for torsion and out-of-plane torsion interactions (Eqs. (2)–(5)).

$$u_r = D_e\left\{\left[1 - e^{-\beta(r-r_0)}\right]^2 - 1\right\} \tag{2}$$

$$u_\theta = \frac{1}{2}k_\theta(\theta-\theta_0)^2\left[1 + k_{sextic}(\theta-\theta_0)^4\right] \tag{3}$$

$$u_\phi = \frac{1}{2}k_\phi[1+\cos(n\phi-\phi_0)] \tag{4}$$

$$u_\omega = \frac{1}{2}k_\omega[1+\cos(n\omega-\omega_0)] \tag{5}$$

As indicated in Figs. 1a and 2, a nonlinear axial spring is used for modeling of the angle variation interaction between atoms. The relationship between changes in the bond and the corresponding change in length of the spring for small displacements can be expressed simply by Eq (7) [15]

$$\Delta\theta \approx \frac{2(\Delta R)}{r_0}, r_0 = 0.142\,\text{nm} \tag{6}$$

Therefore, we can simplify Eq. (3)–Eq. (7).

$$u_\theta = \frac{2}{r_0^2}k_\theta(R-R_0)^2\left[1 + \frac{16}{r_0^4}k_{sextic}(R-R_0)^4\right] \tag{7}$$

The stretch force, the angle variation moment, the dihedral angle torque, and out-of-plane torque can be obtained from differentiations of (Eqs. (2), (7), (4), (5)) as functions of bond stretch, bond angle, dihedral angle, and out-of-plane angle variation, respectively:

$$F(r-r_0) = 2\beta D_e\left[1 - e^{-\beta(r-r_0)}\right]e^{-\beta(r-r_0)} \tag{8}$$

$$F(R-R_0) = \frac{4}{r_0^2}k_\theta(R-R_0)[1 + \frac{16}{r_0^4}(1+\frac{4}{r_0^2})k_{sextic}(R-R_0)^4] \tag{9}$$

$$T(\phi-\phi_0) = \frac{1}{2}k_\phi n\sin(n\phi-\phi_0) \tag{10}$$

$$T(\omega-\omega_0) = \frac{1}{2}k_\omega n\sin(n\omega-\omega_0) \tag{11}$$

A nonlinear connector is considered for modeling of the stretching and torsional interactions and a nonlinear spring for modeling of the angle variation interaction (see Fig. 2). Carbon atoms in ABAQUS are modeled by a discrete rigid sphere so that connector elements between toms are adjoined to reference points at the center of the sphere and a local coordinate is set at the center of each atom (see Figs. 1b and 2). This local coordinate is a combination of a Cartesian coordinate for stretching and a rotational coordinate for torsion. The X direction of these coordinates is in the connector direction, and the Z direction is vertical to the central axis of the nanotube. Because we can only use a linear spring in the CAE space of ABAQUS, by changing the linear spring command to a nonlinear spring command in the input file, and by applying the nonlinear data for $F(\Delta R)$ versus ΔR using Eq. (9), we can apply the bond bending spring to the model. For applying bond stretch and torsion forces to the connectors, we can apply the nonlinear stiffnesses in three directions (X, Y, Z) directly. For stretching stiffness in the X direction, we can obtain the nonlinear data for $F(\Delta r)$ versus Δr by Eq. (8), and for torsional stiffness in X direction, we can obtain the nonlinear data for $T(\Delta\phi)$ versus $\Delta\phi$ by Eq. (10). For torsional stiffness in the Y direction, we can

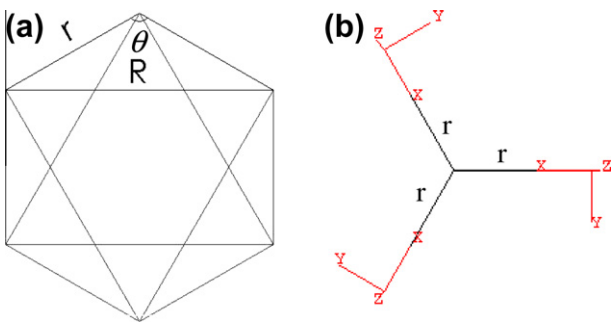

Fig. 1. (a) A hexagonal unit cell, (b) location of local coordinates of each connector.

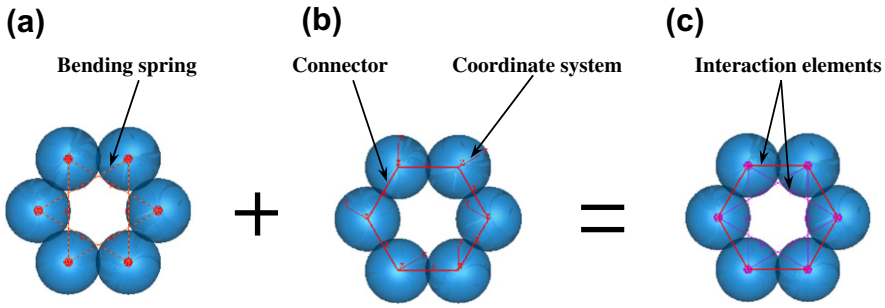

Fig. 2. Spring and connector elements corresponding to the interactions of carbon atoms. (a) The angle variation interactions, (b) the stretching and torsional interactions, (c) total interactions.

obtain the nonlinear data for $T(\Delta\omega)$ versus $\Delta\omega$ by Eq. (11). Here, we take $E = 1170$ GPa and $v = 0.196$ for the Young's modulus and Poisson's ratio of single-walled carbon nanotubes, respectively. As shown in our previous work, we used $k_r = 800$ nN/nm, $k_\theta = 1.42$ nN/nm Rad^{-2}, $k_\varphi = k_\omega = 0.0418$ nN nm, which are consistent with the values reported in the literature. In order to include the inertia effects, the mass of each carbon atom is assumed as a mass point (1.9943×10^{-26} kg) at nodes coinciding with carbon atoms. The masses of electrons, connectors and springs are neglected and individual atoms acting as concentrated masses at the joints in the structure.

This structural model was successfully used for predicting the mechanical properties and axial buckling behavior of single-walled carbon nanotubes. It is employed here for predicting the natural frequency of single-walled carbon nanotubes.

3. Results and discussion

In this section, the commercial finite element numerical package ABAQUS was used to study the natural frequency of a fixed–fixed and free–fixed SWCNT. The natural frequencies were predicted with the present structural model. Zigzag and armchair SWNTs with various aspect ratios (L/D) were employed for this study. The effect of different types of defects (vacancies and Stone–Wales) on the natural frequency was also studied for zigzag and armchair nanotubes with various aspect ratios. Fig. 3a shows the natural frequencies of perfect nanotubes with different aspect ratios and fixed–fixed boundary conditions. The natural frequencies were obtained with our model and are compared with results from K. Hashemnia et al. [10]. It can be seen that when the Euler mode occurs, results are in good agreement with each other. However, when the shell mode occurs, the predicted frequencies of Hashemnia et al. are greater than our results. This difference was not seen for results with fixed–free boundary conditions (see Fig. 3b).

The results of the present model are identical to the work of Duan et al. [16] using molecular dynamics; however, they did not obtain results for small aspect ratios and defective nanotubes (Table 1). As mentioned before, CNTs with a small aspect ratio are often used for NEMS.

In Fig. 4, we compare the present results to those from the simple continuum model (with a wall thickness of 0.066 nm reported by Yakobson et al. [17]) in ABAQUS software. The mass of nanotube is assumed equal to the mass of all carbon atoms in the SWCNTs. The natural frequencies were logarithmically plotted as function of aspect ratios. The predicted FEM results by a continuum model and fixed–fixed and fixed–free end conditions are much greater than our results and those of Hashemnia et al. when the shell mode occurs. The main reason for this difference is the different behavior of the nanotubes in the shell and Euler modes. SWCNTs can most likely be modeled as continuum tubular shells when the Euler mode occurs, but it is impossible to model those by continuum models when the shell mode occurs. A comparison between the FEM results and the proposed model shows that the continuum model cannot completely predict the exact natural frequencies of CNTs. When the shell mode occurs, the natural frequencies predicted by FEM are higher, and when the Euler mode occurs, they are lower than values obtained by the proposed model. However, a cylindrical tube continuum with a wall thickness equal to 0.066 nm can generally predict the average of the results (within 2 nm < L/D < 12 nm).

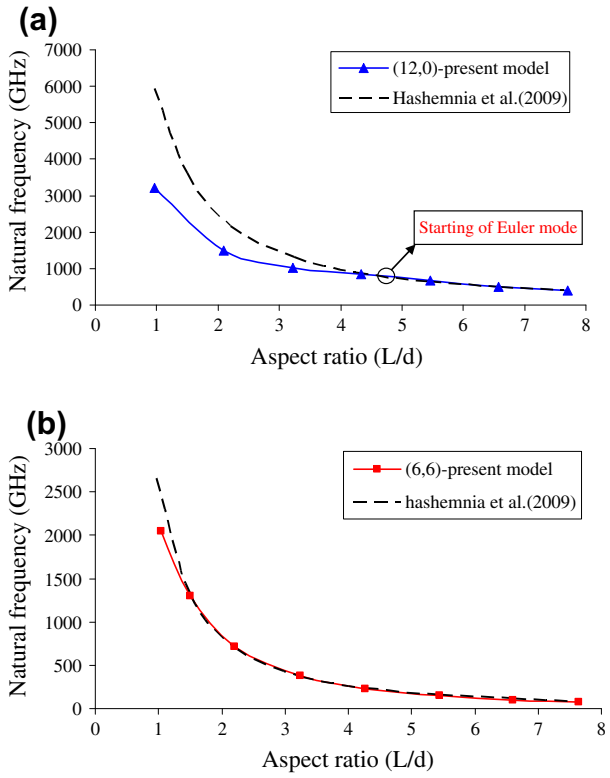

Fig. 3. Comparison the present results to previous results of the beam structural method for (12, 0) SWCNTs with fixed–fixed (a) and fixed–free (b) boundary conditions (influence of the aspect ratio of SWCNTs on the natural frequencies).

The present model is a good model to investigate the effects of various defects on natural frequencies. The types of vacancy defects for the study of defects in carbon nanotubes are illustrated in Fig. 5. Vacancies result from missing carbon atoms in the CNT walls. The defects included are single vacancies (one atom missing), double vacancies (two adjacent atoms missing) and triple vacancies (three adjacent atoms missing). Stone and Wales showed

Table 1
Natural frequencies (GHz) from the present model and MD model.

Aspect ratio	Fixed–fixed		Fixed–free	
	Present model	W.H. Duan (2007)	Present model	W.H. Duan (2007)
5.26	983	975	216	212
6.35	747	741	154	150
7.07	634	628	126	123
8.16	505	500	97	94
9.25	411	406	76	74
10.34	341	336	63	60
11.43	286	282	51	49
12.52	244	240	42	41
13.6	209	206	34	35

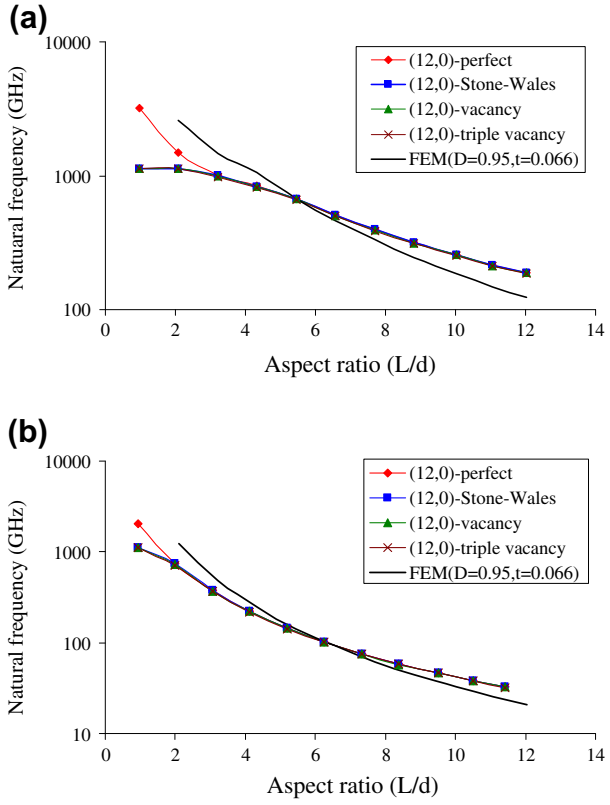

Fig. 4. Natural frequencies vs. aspect ratio of perfect and defective SWCNTs with (a) fixed–free and (b) fixed–fixed boundary conditions.

that a dipole consisting of a pair of 5–7 rings can be created by rotating the C–C bond in a hexagonal network by 90°. As shown in Fig. 6, in this rotation, four hexagons are changed into two heptagons and two pentagons. Here, we suppose that an initial Stone–Wales defect exists on the nanotube before the tension test (see Fig. 6). All of the defects are situated in the middle of the nanotube.

As indicated in Fig. 4, the defects have a very weak effect on the natural frequencies when the Euler mode occurs. Of course, it should be noted that for defective nanotubes, the Euler mode will occur later; it occurs at an aspect ratio of approximately 4.5 for vacancy and Stone–Wales defects while for double and triple vacancies, it occurs at an aspect ratio of 5.5 and 6, respectively. However, based on the present results, the effect of defects on these carbon nanotubes will be critical when the shell mode occurs. Therefore, to use carbon nanotubes with the small aspect ratios, we should use perfect ones.

When the shell mode occurs, the vibrational mode shapes of defective CNTs are completely affected by defects. Contrary to what is assumed, the effect increases slightly with increasing defects. Furthermore, the Stone–Waals defects, which are due to retaining the inter-atomic bonds, are assumed to have less effect compared to vacancy defects on the natural frequencies, but it is not true. It seems that in the vibrational frequency domain the smallest change in the material structure at local modes can cause great changes in the natural frequencies. Furthermore, tube chirality does not have a significant effect on the natural frequency of SWCNTs.

The mode shapes according to the displacement contours are represented for two lengths of perfect and defective nanotubes with fixed–fixed boundary conditions in Fig. 7. With increasing length of nanotubes, the shell mode shapes convert to the Euler mode shape. The difference between the shell mode shapes of perfect and defective nanotubes confirm the difference between the natural frequencies for CNTs with small aspect ratios.

The rate of natural frequency reduction is greater for lower aspect ratios due to the increase of the aspect ratio and diameter, which indicates that the effect of the diameter on the natural frequencies is greater for lower aspect ratios. This issue causes

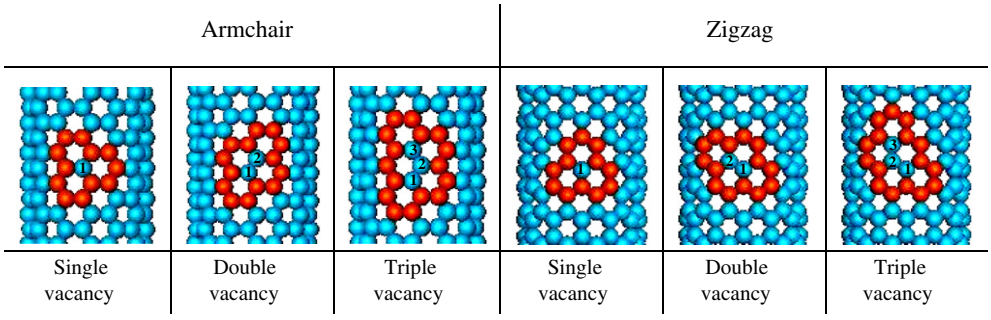

Fig. 5. Different vacancy defects used in analysis (removed carbon atoms indicated by numbers).

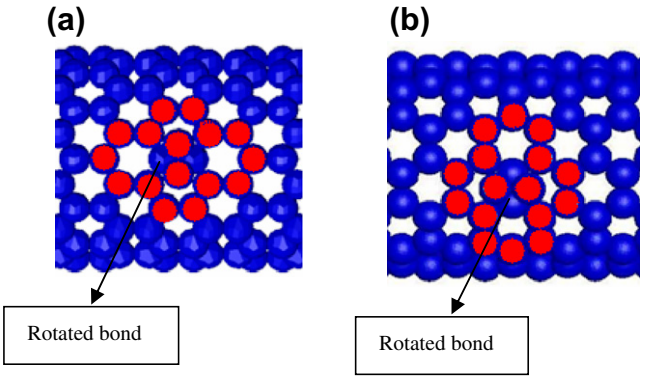

Fig. 6. Configuration of Stone–Wales defects in zigzag (a) and armchair (b) nanotubes (indicated in red colour). (For interpretation of the references to colour in this figure legend, the reader is referred to the web version of this article.)

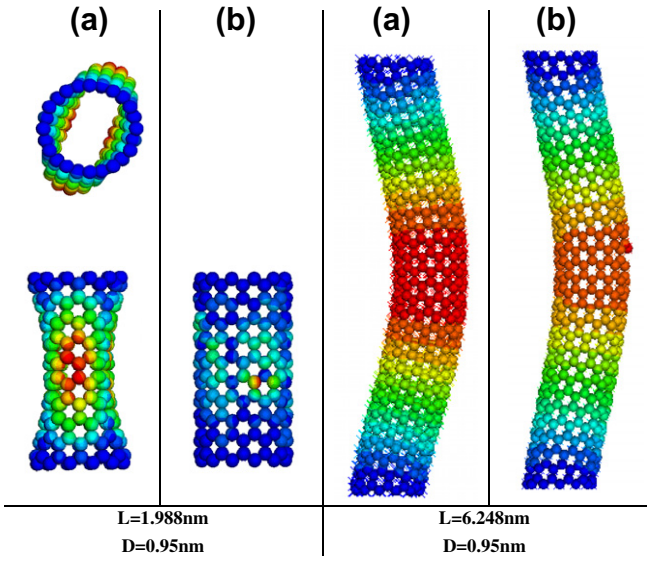

Fig. 7. The mode shapes of (12, 0) SWCNTs under frequency analysis: (a) perfect and (b) defective.

access to a variety of frequencies, which is useful for NEMS.It should be noted that the natural frequencies are affected by their mode shape and the position of the defect on nanotube length. The frequency shift (Δf), is then represented by Eq (1):

$$\Delta f = f_{per} - f_{def} \tag{12}$$

where f_{per} denotes the fundamental frequency of the perfect nanotube and f_{def} indicates the fundamental frequency of the defected nanotube.

Fig. 8 shows curves of the shift of fundamental frequencies versus the displacement of defect along the nanotube for fixed–fixed and free–fixed boundary conditions. The locations of the single vacancy defect are situated at $L_0 = 0.1L$, $0.25L$, $0.5L$, $0.75L$ and $0.9L$, where L_0 is the distance of the defect from the fixed end and L is the length of the nanotube. Results indicate that with displacement of the defect toward the free end of the nanotube, the reduction of the shift of fundamental frequencies will become minor (see Fig. 8a); hence, the critical points for the existence of the defect are near the fixed end of the carbon nanotube. As shown in Fig. 8b, It is noticed that the critical points for the existence of the defect are near the fixed ends when shell mode occurs ($L/D < 5$); however this critical point is at the middle of nanotube when Euler mode occurs.

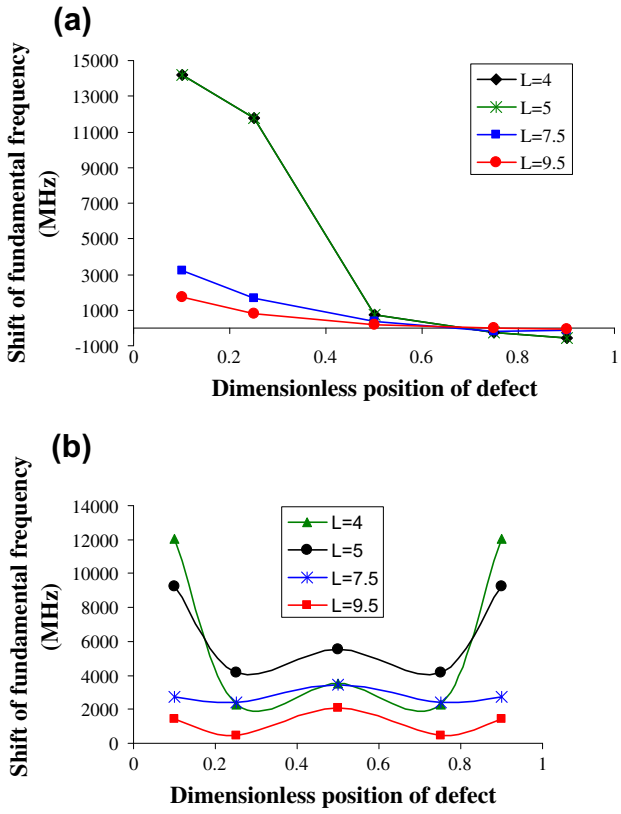

Fig. 8. Fundamental frequency shift of (12, 0) SWCNT with different lengths versus position of vacancy defect (a) free–fixed end and (b) fixed–fixed end.

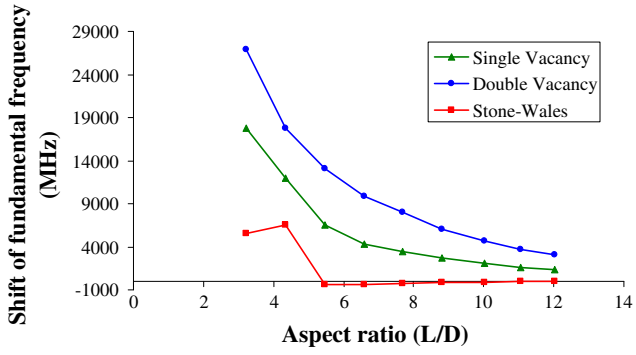

Fig. 9. Influence of defects on the fundamental frequency shift with variation of nanotube aspect ratio and fixed–fixed boundary conditions.

Fig. 9 shows the shift of fundamental frequency of (12, 0) SWCNT with vacancies and Stone–Wales defect versus the aspect ratios of nanotube. It is easy to understand that single vacancy is superior to double vacancies for (12, 0) tube, because defective area induced by the single vacancy is obviously smaller. But the frequency of defective nanotube including Stone–Wales defect is larger than that of perfect one when Euler mode occurs. The shift of frequency of SWCNT decreases with increase in aspect ratio.

4. Conclusion

The effects of the type of vacancy and Stone–Wales defects on the vibrational behavior of SWCNTs under frequency analysis were studied based on a structural mechanics approach using ABAQUS software. Our results show that the structural models with beam

elements cannot most likely predict the natural frequency for small aspect ratios of nanotubes exactly. For all of the structural models that were used for the prediction of the natural frequencies, we needed to select a sufficiently long nanotube. This option is more sensitive for fixed–fixed boundary conditions.

Defects do not have a significant effect on the natural frequencies of sufficiently long SWCNTs. However, for nanotubes with shorter lengths, this effect is much greater (aspect ratio of approximately 4.5 and up). CNTs with the small aspect ratios are often used for NEMS due to their high frequencies. Therefore, it is necessary to use an exact prediction because of the occurrence of the shell modes at this range. With displacement of the defect toward the free end of the fixed–free nanotube, the reduction of the shift of fundamental frequencies will become minor; however maximum shift of fundamental frequency is at the middle of fixed–fixed nanotube when Euler mode occurs. Furthermore, the frequency of defective nanotube including Stone–Wales defect is larger than that of perfect one when Euler mode occurs.

Reference

[1] R.F. Gibson, E.O. Ayorinde, Y.F. Wen, Composites Science and Technology 67 (2007) 1–28.
[2] D.H. Wu, W.T. Chien, C.S. Chen, H.H. Chen, Sensors and Actuators A 126 (2006) 117–121.
[3] J.C. Hsu, R.P. Chang, W.J. Chang, Physics Letters A 372 (2008) 2757–2759.
[4] Y.W. Kwon, C. Manthena, J.J. Oh, D. Srivasta, Journal of Nanoscience and Nanotechnology 5 (2005) 703–712.
[5] K.Y. Xu, E.C. Aifantis, Y.H. Yan, Journal of Applied Mechanics, Transactions ASME 75 (2008) 0210131–0210139.
[6] S.K. Georgantzinos, N.K. Anifantis, Computational Mechanics 47 (2009) 168–177.
[7] S.K. Georgantzinos, N.K. Anifantis, Physica E 42 (2010) 1795–1801.
[8] C. Li, T.W. Chou, Physical Review B 68 (2003) 073405.
[9] R. Chowdhury, S. Adhikari, C.Y. Wanga, F. Scarpa, Computational Materials Science 48 (2009) 730–735.
[10] K. Hashemnia, M. Farid, R. Vatankhah, Computational Materials Science 47 (2009) 9–85.
[11] M. Mir, A. Hosseini, G.H. Majzoobi, Computational Materials Science 43 (2008) 540–548.
[12] A. Sakhaee-Pour, M.T. Ahmadian, A. Vafai, Thin-Walled Structures 47 (2009) 646–652.
[13] V. Parvaneh, M. Shariati, A.M. Majd Sabeti, European Journal of Mechanics A/Solid 28 (2009) 1072–1078.
[14] A.K. Rappe, C.J. Casewit, K.S. Colwell, et al., Journal of American Chemical Society 114 (1992) 10024–10035.
[15] G.M. Odegard, T.S. Gates, L.M. Nicholson, K.E. Wise, NASA/TM (2002) 211454.
[16] W.H. Duan, C.M. Wang, Y.Y. Zhang, Journal of Applied Physics 101 (2007) 024305.
[17] B.I. Yakobson, C.J. Brabec, J. Bernholc, Physical Review Letters 76 (1996) 2511–2514.